Kinetics of ion-induced ripple formation on Cu(001) surfaces

Wai Lun Chan, Niravun Pavenayotin, and Eric Chason
Division of Engineering, Brown University, Providence, Rhode Island 02912, USA
(Received 23 February 2004; published 25 June 2004)

We have used low energy ion beams to spontaneously create patterns (sputter ripples) on Cu(001) surfaces. The evolution of the ripple amplitude and wavelength was measured *in situ* by using light scattering. At the temperatures (415–455 K) and ion fluxes (10^{14}–10^{15} ions cm^{-2} s^{-1}) studied, the ripple formation process is found to be similar to that described by the Bradley-Harper instability theory, i.e., the wavelength does not change appreciably with time, the orientation is determined by the ion beam direction and the amplitude increases exponentially during the early stages of growth. The flux dependence of the growth rate and wavelength is measured to determine the kinetics of defect production and annihilation on the surface.

DOI: 10.1103/PhysRevB.69.245413 PACS number(s): 79.20.Rf, 68.35.Bs, 61.80.Jh

I. INTRODUCTION

Spontaneous pattern formation on surfaces due to low-energy ion bombardment is a well-known phenomenon.[1,2] Ripples, mounds or pits with length scales ranging from microns to tens of nanometers have been observed to form in many different systems including amorphous materials,[3] semiconductors,[4–7] graphite,[8] and metals.[9–14] A variety of pattern-forming behavior has been observed depending on the substrate, the ion beam, the angle of incidence, and other processing parameters. In some cases, the wavelength is nearly constant with fluence[3–5] while in others the wavelength increases with sputtering time.[9,11,13] The patterns align with the ion beam direction under some conditions,[3–5,14] while under others it is determined by the orientation of the surface.[10,12]

In this work, we report on the use of low energy ion beams to create sputter ripples on Cu(001) surfaces. The ripple formation kinetics were measured using *in situ* light scattering[15] so that we could simultaneously determine the ripple wavelength and amplitude during sputtering. We present measurements of the time evolution of the ripple wavelength and amplitude and the dependence of the ripple on the ion beam direction and the surface crystallographic orientation. Measurements of the dependence of the wavelength and growth rate on ion flux are also presented.

Our measurements indicate that the ripple wavelength is essentially constant during growth, the amplitude grows exponentially in the early stages and the orientation is determined by the ion beam direction. These results are consistent with an instability formation mechanism proposed originally by Bradley and Harper[16] (BH) and previously observed on other surfaces.[3–5] This is the first time that the ripple growth on a metal surface has been shown quantitatively to have the features of a BH instability. We analyze the ion flux dependence of the wavelength and growth rate in terms of this theory to determine the kinetic mechanism for defect production and annihilation.

II. MODELS OF SPUTTER RIPPLE FORMATION

The BH model was originally proposed to explain the observation of periodic patterns measured by scanning electron microscopy after long sputtering times. The primary features of these patterns were that they were produced spontaneously and their direction was determined by the incident ion beam direction. In addition, as the angle of incidence was decreased from near normal to near grazing incidence, the orientation of the pattern was observed to rotate by 90° with respect to the projected direction of the ion beam on the surface.

The BH model combines surface roughening due to ion-induced atom removal with a surface smoothing mechanism due to diffusion. The surface roughening rate was based on a sputtering model proposed by Sigmund[17] in which the sputter yield depends on the local surface morphology so that the rate of surface erosion is curvature dependent. Surface smoothing was explained using an approach developed by Herring and Mullins[18] in which surface curvature induces gradients in the chemical potential to drive surface diffusion. Cuerno and Barabasi (CB) extended the BH theory by adding higher order nonlinear terms[19] which prevent the ripple from growing indefinitely. The resulting equation for the evolution of the surface height is given by

$$\frac{\partial h}{\partial t} = -\nu_0 + \frac{\partial \nu_0}{\partial \theta}\frac{\partial h}{\partial x} + \nu_x \frac{\partial^2 h}{\partial x^2} + \nu_y \frac{\partial^2 h}{\partial y^2} + \frac{\lambda_x}{2}\left(\frac{\partial h}{\partial x}\right)^2 + \frac{\lambda_y}{2}\left(\frac{\partial h}{\partial y}\right)^2 - B\nabla^2\nabla^2 h, \quad (1)$$

where ν_0 is the erosion rate in terms of the incident angle θ, and ν_x, ν_y, λ_x, and λ_y are coefficients calculated in Ref. 2. B, the coefficient that describes diffusional smoothing,[18] is equal to $D_s \gamma C / n^2 k_B T$ where D_s is the surface diffusivity, γ is the surface free energy, C is the concentration of mobile species, and n is the areal concentration of atomic sites.

In the early stages of ripple formation, the different spatial dependence of the roughening and smoothing processes results in an instability, i.e., the selection of a preferred spatial periodicity that grows faster than all others. The wave vector of the fastest growing Fourier component k^* depends on the ratio of the sputter roughening rates and the diffusional relaxation rate,

$$k^* = \left(\frac{\nu_{\max}}{2B}\right)^{1/2}, \quad (2)$$

where $\nu_{\max}$ is the larger of the two values $-\nu_x$ and $-\nu_y$. The amplitude grows exponentially at this wave vector as $\exp(R^*t)$ where $R^* = (\nu_{\max})^2/4B$. Since the parameter B is related to the surface diffusivity and mobile defect concentration, the surface kinetics are directly linked to the wavelength of the resulting pattern. At longer sputtering times, nonlinear terms become significant so that the amplitude may saturate and the wavelength may not remain fixed.

Effects of surface crystallinity are not included in the BH theory so that the orientation of the ion beam relative to the surface lattice parameters does not enter into the theory. The wave vector of the ripple pattern created by the instability is either aligned parallel to the ion direction or perpendicular to it depending on the parameters ν_x and ν_y. These parameters are completely determined by the incident ion beam through the ion–solid interaction and the angle of incidence. However, in some systems (primarily metals) the surface pattern is found to be aligned along surface crystallographic directions independent of the ion beam direction.[10] Rusponi *et al.*[9,10] proposed a diffusion-based roughening mechanism originating from the presence of Schwoebel barriers, adapted from a model proposed by Villain[20] for the morphology of crystal growth. In Villain's model, supersaturated adatoms (either from growth beam or sputtering) on a high symmetry surface prefer to stick to the edge of the upper terraces rather than the lower ones because of the Schwoebel barrier. This results in a net uphill adatom current that induces surface roughening. The strength of this mechanism depends on both the fraction of adatoms that attach to the step edge and the degree of biasing in attachment. This mechanism has been proposed to explain the evolution of patterns on sputtered Cu(110) surfaces[9,10] in which the pattern is aligned with the surface symmetry.

Since at high temperature the steps are less effective sinks for adatom and the degree of biasing is less, the roughening mechanism due to diffusion effects is expected to decrease at higher temperature. Moreover, the roughening from the curvature-dependent sputter yield in the BH model increases with the ion flux. In this work, higher fluxes and temperatures were used relative to previous studies of single crystal Cu surfaces[9,10,14] in order to promote the instability mechanism relative to diffusional mechanisms.

III. EXPERIMENTAL DETAILS

Experiments were performed on Cu(001) surfaces with miscut less than 1° inside an ultrahigh vacuum chamber with base pressure of 4×10^{-9} torr. Samples were polished by an electrochemical method[21] before each run. AFM studies show that the rms roughness after polishing was typically less than 10 Å over a 10 μm $\times$ 10 μm region. After transfer into the vacuum system, the sample was cleaned at room temperature by Ar^+ sputtering at normal incidence. In this procedure, approximately 1000 monolayers of copper were removed. The sample was then annealed at 700 K to eliminate any fine scale roughness resulting from the step above. The sputter source was a Kaufmann-style ion gun. Sputtering was done in an Ar atmosphere with a nominal pressure of 1.5×10^{-4} torr. Unless otherwise noted, rippling was done with an ion beam energy equal to 800 eV, the angle of incidence θ of the beam was set at an angle 70° from the normal of the sample surface and the direction of the beam projected onto the surface was along the [100] direction. Experiments were performed at temperatures in the range from 415 K to 455 K with ion fluxes in the range from 1.1 to 3.4×10^{14} ions cm^{-2} s^{-1}.

The evolution of the power spectral density (PSD) of the sample surface was measured in real time by a spectroscopic light scattering technique referred to as LiSSp.[15] In this method, the scattered intensity is measured by a spectrometer as a function of wavelength at a fixed scattering angle which enables the entire PSD to be obtained without rotating the sample or the detector. Periodicity in real space from 300 to 2000 nm can be studied using our present setup by simultaneously collecting spectra at several different scattering angles with respect to the sample surface.

The PSD is proportional to the scattered power at each scattering vector with a constant of proportionality determined by Elson in Ref. 22. Although this constant of proportionality can be calculated, in practice it is simpler to normalize the scattered intensity by the intensity measured on the smooth starting surface. Since the scattered intensity is proportional to the surface PSD, the resulting intensity ratio is equal to the ratio between the PSD of the sputtered surface and the starting smooth surface. In this way, detailed knowledge of the optical constants and other parameters required to calculate the proportionality between the intensity and the PSD is not required to analyze the data.

The light source was a 150 W Xe arc lamp. Spectra were typically acquired every 30 minutes. Sputtering was paused for several minutes during measurement of the spectra in order to minimize coating of the optical viewports by material sputtered from the sample. Measurements show that the ripple amplitude deceases by less than 4% during a 30 minute pause, so the decrease in ripple amplitude during the few minutes required for measurement has a negligible effect on the surface morphology.

IV. RESULTS AND DISCUSSIONS

A. Time evolution of the ripples

Figure 1(a) shows the evolution of the normalized PSD during sputtering at 418 K with an ion flux of 2.1×10^{14} ions cm^{-2} s^{-1}. The peak in the data, at a value of wave vector $k=0.016$ nm^{-1}, corresponds to a surface modulation with a real space wavelength of approximately 393 nm. The error in wavelength is determined from the standard deviation of the peak value over 20 experimental runs under one set of sputtering conditions; the same percentage error is used for the values measured at different flux and temperature. AFM images of the same sample after sputtering are shown in Fig. 1(b). These measurements indicate a ripple wavelength of 400 nm $\pm$ 20 nm with the same orientation relative to the ion beam, in good agreement with the light scattering measurements. The wavelength of the ripples

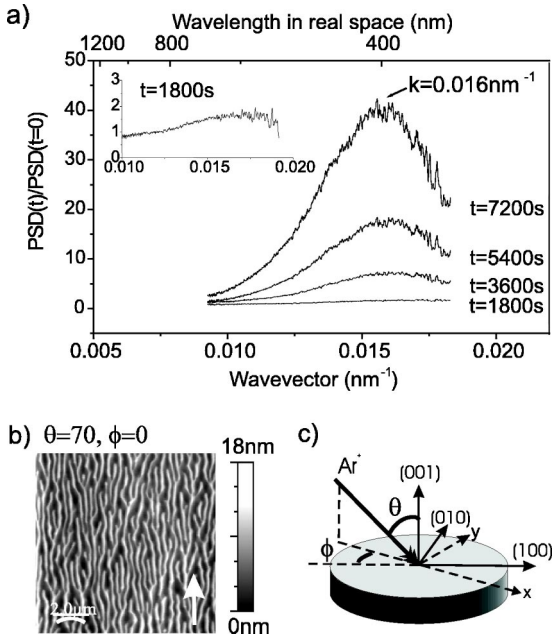

FIG. 1. (a) Time evolution of power spectral density (PSD) of the sample surface during sputtering. The sputtering temperature is 418 K and ion flux is 2.1×10^{14} ions cm^{-2} s^{-1}. The ion beam is oriented 70° away from normal with a direction parallel to the [100] axes. (b) AFM images of the sputtered ripples (the arrow indicates the direction of the ion beam). (c) Schematic diagram showing the sputtering geometry.

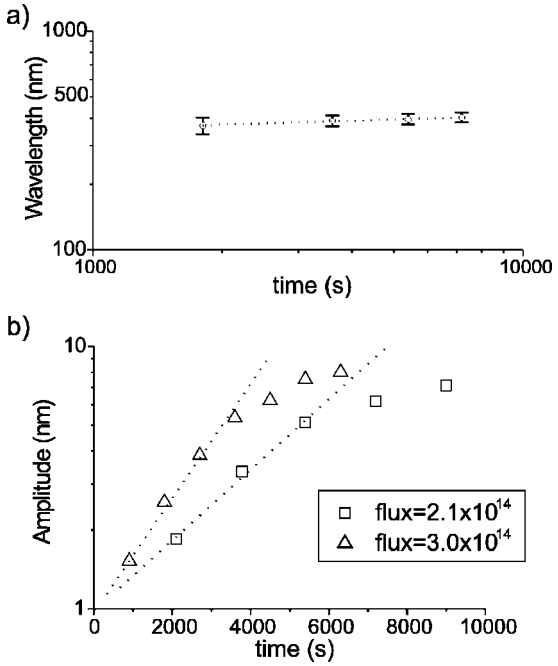

FIG. 2. (a) Ripple wavelength vs sputtering time of the data shown in Fig. 1. The dotted line shows a power law fit with an exponent of 0.06. (b) Ripple amplitude vs sputtering time. The samples temperature is 418 K, with ion flux equal to 2.1×10^{14} (square) and 3.0×10^{14} ions cm^{-2} s^{-1} (triangle). The dotted lines in the figure correspond to exponential growth.

as a function of time is shown in Fig. 2(a). The wavelength is essentially constant with ion fluence, changing by less than 10% over a factor of 4 in the increase in sputtering time. When fit to a power law, the exponent is equal to 0.06 ± 0.005.

From a series of spectra acquired during sputtering, the time dependence of the amplitude of the ripples is obtained as shown in Fig. 2(b). Two sets of data are shown, taken at fluxes of 2.1×10^{14} and 3.0×10^{14} ions cm^{-2} s^{-1} and at a temperature of 418 K. In both cases, the amplitude of ripples grows exponentially in the early stages but saturates at longer times. This behavior is similar to measurements on Si(001) surfaces[23] and consistent with the nonlinear BH theory proposed by Cuerno and Barabasi.[19] The dashed lines represent the results of least square fits to the data to determine the rate of exponential growth in the early stages. The maximum growth rate of the ripples for the flux of 2.1×10^{14} ions cm^{-2} s^{-1} is on the order of 0.0022 nm s^{-1}. For comparison, the average rate of erosion of the surface is measured to be 0.068 nm s^{-1} by using *ex situ* profilometry.

B. Orientation of the ripples

In this section, we present and discuss measurements of sputter ripple orientation as a function of the direction of the ion beam projected onto the surface (azimuthal orientation ϕ) and angle of incidence θ relative to the surface normal. The meaning of these angles with respect to the orientation of the sample is shown in Fig. 1(c).

1. Azimuthal orientation

AFM measurements of sputter ripples produced at different azimuthal orientations are shown in Fig. 3. In each image, the sample has been rotated in 15° increments around the surface normal so that the ion beam is parallel to the [100] direction in Fig. 3(a) and parallel to the [110] direction in Fig. 3(d). The arrows in the figure indicate the orientation of the sample ⟨100⟩ axes and the direction of the ion beam projected onto the surface. The small images below each AFM image represent the two-dimensional (2D) autocorrelation function of the data; a cross section of the autocorrelation function along the direction of the ripple wave vector is presented at the bottom. The angle of incidence is the same ($\theta=70°$) for all of the measurements. The beam energy was 800 eV, sample temperature was 418 K and the flux was 2.1×10^{14} ions cm^{-2} s^{-1}.

In Figs. 3(a) and 3(d) the ion beam is parallel to major crystallographic directions and the wave vector of the pattern is very well aligned normal to the direction of the ion beam projected onto the surface. In the case of 15° misalignment relative to the [100] axis [Fig. 3(b)], there is a tendency for some of the pattern to remain aligned along the [100] crystallographic axes as well as with the ion beam direction. For 30° misalignment [Fig. 3(c)], the pattern is mostly aligned along the ion beam direction, although branches of ripples along [100] direction are also found. In addition, for Figs. 3(b) and 3(c) the higher order peaks in the autocorrelation function are blurred, indicating a decrease in the alignment of the ripples.

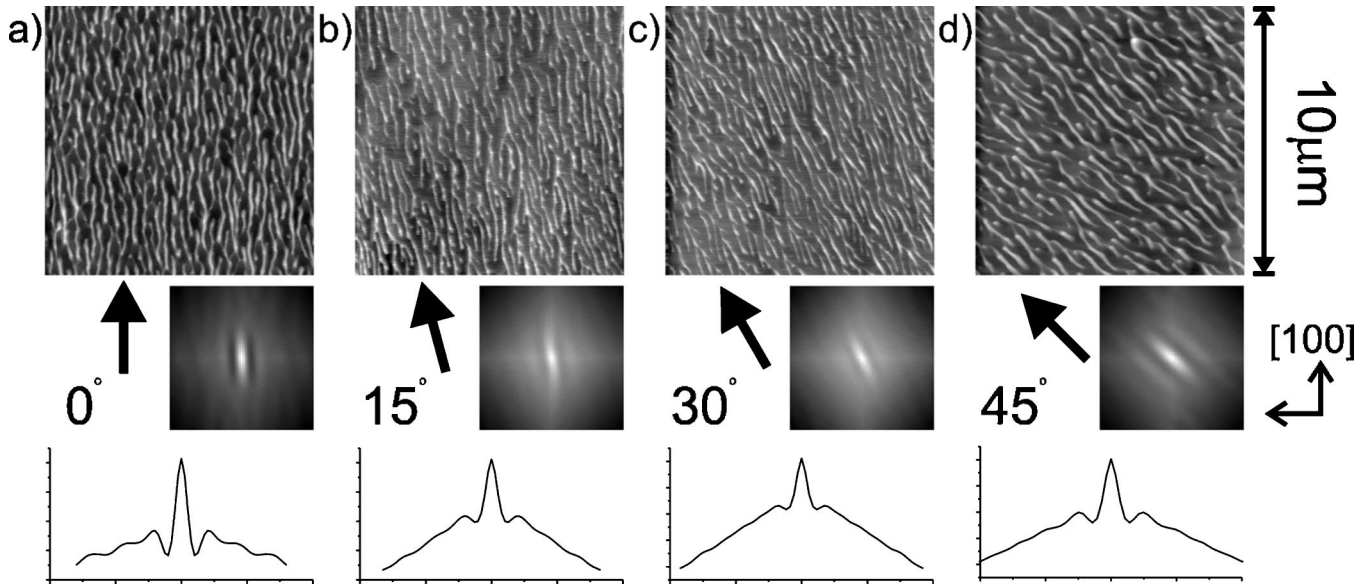

FIG. 3. AFM images of the sputtered surfaces at different ion beam directions. The sputtering conditions are the same as Fig. 1 and the total ion fluence is 2.3×10^{18} ions cm^{-2}. The wide arrows below each figure indicate the direction of the ion beam; the [100] direction is indicated by the labeled arrows. The angle between the ion beam and the [100] direction for (a), (b), (c), (d) are 0°, 15°, 30°, 45°, respectively. The small figure below each image shows the 2D autocorrelation function. The graph at the bottom is a cross section of the autocorrelation function along the direction parallel to the ripples wave vector.

These images indicate that the alignment of the sputter ripple pattern is determined primarily by the direction of the ion beam, behavior that is consistent with the BH model. Since the BH theory does not include any effects of surface crystallography, the pattern is not predicted to depend on the azimuthal orientation of the surface. However, there is some evidence in the off-axis results that the underlying crystal orientation does affect the pattern formation. The small tendency of the ripples in Figs. 3(b) and 3(c) to align preferentially in the [100] and [110] direction may be related to the effect of diffusional mechanisms such as the Schwoebel barrier on the pattern formation. Alternatively, these results may indicate the importance of step edge energies on the ripple formation, a topic which is being considered further and will not be addressed here.

2. Angle of incidence

The prediction of a 90° rotation of the pattern as the incident angle of the ion beam changes is a major feature of the BH theory. At large angles of incidence (i.e., closer to grazing incidence), the parameters ν_x and ν_y in Eq. (1) have the form $\nu_x>0$ and $\nu_y<0$ where x is the direction of ion beam. Since ripples only grow for negative values of ν_x and ν_y, a ripple pattern with wave vector in the y-direction (perpendicular to the projected direction of the ion beam) surface is formed. As the angle of incidence decreases toward normal incidence, ν_x decreases much faster than ν_y. At sufficiently low angles, ν_x and ν_y are both negative and the absolute value of ν_x is greater than ν_y. In this case, roughening occurs along the ion beam direction (x direction) faster than in the direction orthogonal to it. As a result, ripples form with their wave vector parallel to the direction of ion beam and the pattern rotates 90°.

The dependence of the pattern orientation on the incidence angle is shown in the AFM images in Fig. 4. In Fig. 4(a), the incidence angle is $\theta=70°$ with a beam energy of 1200 eV. The temperature is 418 K, the ion flux is 2.1×10^{14} ions cm^{-2} s^{-1} and the total fluence is 1.13×10^{18} ions cm^{-2}. The Fourier transform is shown alongside the image. Two peaks are seen in reciprocal space showing that the wave vector of the pattern is oriented perpendicular to the incident ion direction.

The sputtering conditions necessary to obtain the pattern rotation according to the BH theory were obtained by using TRIM[24] to estimate the ion beam parameters and evaluating ν_x and ν_y in Eq. (1). For ion energy of 1200 eV, ν_x and ν_y are predicted to be equal at $\theta=27.3$. To obtain the pattern shown in Fig. 4(b), the incidence angle is therefore decreased to $\theta=24°$. The same temperature and ion flux is used as in Fig. 4(a) and the total fluence is 3.78×10^{17} ions cm^{-2}. The pattern in Fig. 4(b) has a clear component that is rotated 90° relative to the pattern in Fig. 4(a). However, a modulation along the other direction is superimposed on the structure, suggesting that both modes of ripple formation have been produced. In the Fourier transform, an elliptical peak is observed also implying that roughening occurs in both directions. The peaks of the Fourier transform in the direction parallel to the ion beam direction are further away from origin, showing that $\lambda_x<\lambda_y$ which is also consistent with the calculations that indicate $\nu_x<\nu_y<0$ in this regime.

C. Flux dependence of the ripples

Following the approach used in Ref. 4, the flux dependence of the ripple wavelength and exponential growth rate R^* can be used to explore the kinetics of defect production

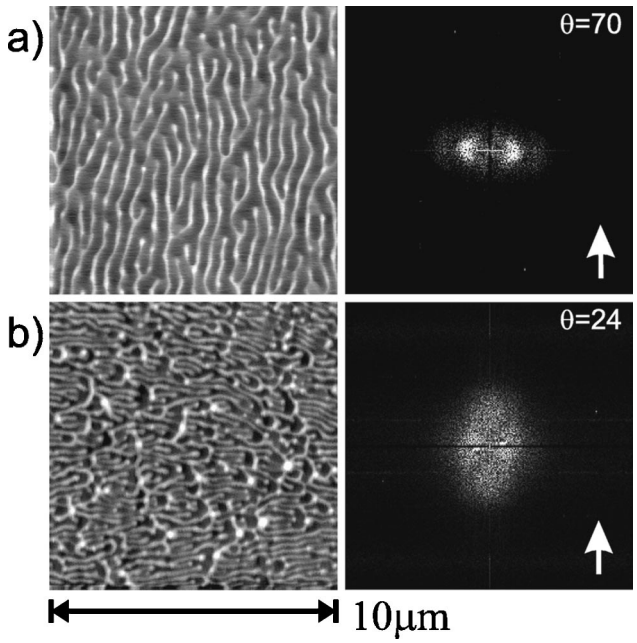

FIG. 4. AFM images of ripples created at (a) $\theta=70°$, ion fluence is 1.13×10^{18} ions cm^{-2}, (b) $\theta=24°$, ion fluence is 3.78×10^{17} ions cm^{-2} and their Fourier transforms. The white arrows represent the direction of the ion beam.

and transport on the surface. As shown in Fig. 5(a), the measured ripple wavelength is independent of flux in the range of 1.1 to 3.4×10^{14} ions cm^{-2} s^{-1} at temperatures of 418 K and 455 K. The significance of this measurement can be understood by examining the flux dependence of the wavelength in Eq. (2). Since $\nu_{\max}$ is proportional to flux f, the peak wavelength is proportional to

$$\lambda^* = \frac{2\pi}{k^*} = 2\pi\left(\frac{2B}{\nu_{\max}}\right)^{1/2} \propto \left(\frac{D_s(T)C(T,f)}{fT}\right)^{1/2}, \qquad (3)$$

where the explicit dependence of each parameter on f and T is written. The observation that the wavelength is independent of f suggests that the ratio D_sC/f is constant with flux. Therefore, the concentration of the diffusing species C is proportional to the ion flux assuming that D_s is independent of flux (i.e., no ion assisted hopping).

We can use this result to determine the mechanism controlling the surface defect concentration using simple rate equations.[4,25] The time dependence of C can be expressed as

$$\frac{\partial C}{\partial t} = Yf - \frac{C}{\tau_1} - 2\frac{C^2}{\tau_2}, \qquad (4)$$

where Y is the net yield of mobile defects created in a single ion impact, τ_1 is a characteristic time for defects to diffuse to a sink such as a surface step, and τ_2 is a characteristic time for two defects to impinge and form a cluster. In steady state, there are different dependences of C on f depending on the relative magnitude of τ_1 and τ_2:

$$C = Yf\tau_1 \text{ for } \tau_1 \ll \tau_2, \qquad (5a)$$

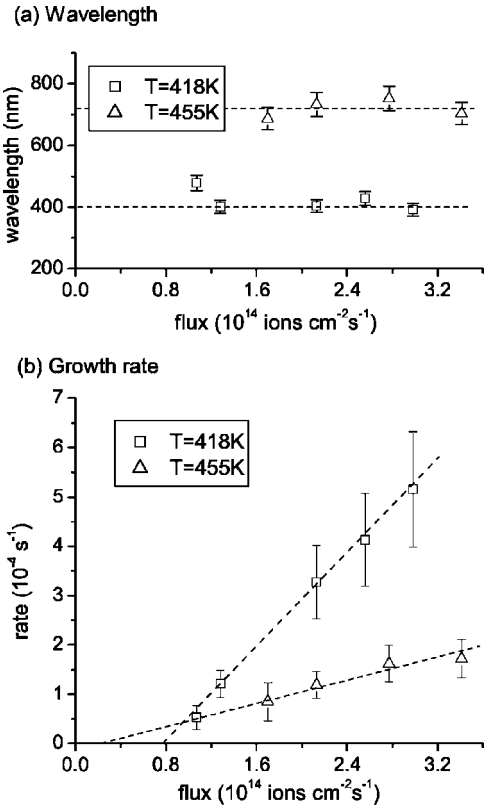

FIG. 5. The flux dependence of (a) ripple wavelength and (b) exponential growth rate of ripples in the early regime. Two sets of data taken at 418 K (square) and 455 K (triangle) are shown. The ripple wavelength is constant with respect to flux within the limit of experimental error. The growth rate varies linearly with flux above a threshold.

$$C = (Yf\tau_2)^{1/2} \text{ for } \tau_2 \ll \tau_1. \qquad (5b)$$

The measured result that C depends linearly on the flux is consistent with the condition that $\tau_1 \ll \tau_2$, i.e., that the surface defect concentration is controlled by annihilation at steps and other sinks. This analysis assumes that the concentration of mobile defects is induced by the ion beam. The flux dependence may change at higher temperature where thermal creation of mobile defects becomes significant.

We can use this dependence of the defect concentration on flux within the BH model to calculate the flux dependence of the ripple growth rate, R^*, in the exponential growth regime. Since $R^*=(\nu_{\max})^2/4B$, this predicts that the growth rate should be proportional to the flux at fixed temperature. The dependence of the measured growth rate on the flux is shown in Fig. 5(b). The growth rate is observed to increase linearly with flux. However, there appears to be a nonzero intercept, i.e., ripples are only produced when the flux is above a threshold value. The appearance of a threshold flux for ripple production is possibly related to the extra energy barrier in creating new steps during roughening, a feature which is not included in the BH theory. However, the observation is consistent with previous studies that at low flux and high temperature regime, the surface remains smooth under the action of an ion beam.[10]

V. CONCLUSION

In summary, we have studied sputter ripple formation on metal surfaces at relatively high temperature and fluxes so that the effects of diffusional barriers were reduced relative to previous studies of Cu surfaces. The measured pattern formation behavior is consistent with the BH instability mechanism. Under these conditions, the ripple wavelength is observed to remain nearly constant with increasing fluence and the amplitude grows exponentially in the early stages. The direction of the pattern is determined by the ion beam direction as predicted by the BH theory. As the angle of incidence decrease from near grazing towards normal, the pattern rotates by 90°. As the azimuthal direction is rotated from along the ⟨100⟩ toward the ⟨110⟩ direction, the pattern rotates with the incident ion direction. Portions of the ripple pattern have a tendency to align along crystallographic directions suggesting the possible presence of other mechanisms not included in the BH theory. The observation that the wavelength is independent of the flux suggests that the concentration of mobile species on the surface is proportional to the flux. This is consistent with the creation of mobile defects by the ion beam and their annihilation at step edges and other sinks.

ACKNOWLEDGMENTS

The authors gratefully acknowledge helpful discussions with Vivek Shenoy and the support of the U.S. Department of Energy under Contract No. DE-FG02-01ER45913. The contributions of Jonah Erlebacher, Gerald Hodgkinson, Meera Shah, Joanna Bettinger, Irene Chang, Frederick Biga, Reese Webb, Kom Promsuttikul, Corrado Boragno, Giovanni Costantini, M. U. Gonzalez, and M. A. Scarpulla to various phases of the project are gratefully acknowledged.

[1] U. Valbusa, C. Borangno, and F. R. de Mongeot, J. Phys.: Condens. Matter **14**, 8153 (2002).
[2] M. A. Makeev, R. Cuerno, and A. L. Barabasi, Nucl. Instrum. Methods Phys. Res. B **197**, 185 (2002).
[3] T. M. Mayer, E. Chason, and A. J. Howard, J. Appl. Phys. **76**, 1633 (1994).
[4] J. Erlebacher, M. J. Aziz, E. Chason, M. B. Sinclair, and J. A. Floro, Phys. Rev. Lett. **82**, 2330 (1999).
[5] E. Chason, T. M. Mayer, B. K. Kellerman, D. T. Mcllroy, and A. J. Howard, Phys. Rev. Lett. **72**, 3040 (1994).
[6] S. Facsko, T. Dekorsy, C. Koerdt, C. Trappe, H. Kurz, A. Vogt, and H. L. Hartnagel, Science **285**, 1551 (1999).
[7] S. Habenicht, K. P. Lieb, J. Koch, and A. D. Wieck, Phys. Rev. B **65**, 115327 (2002).
[8] S. Habenicht, Phys. Rev. B **63**, 125419 (2001).
[9] S. Rusponi, G. Costantini, C. Boragno, and U. Valbusa, Phys. Rev. Lett. **81**, 4184 (1998).
[10] S. Rusponi, G. Costantini, C. Boragno, and U. Valbusa, Phys. Rev. Lett. **81**, 2735 (1998).
[11] M. V. R. Murty, T. Curcic, A. Judy, B. H. Cooper, A. R. Woll, J. D. Brock, S. Kycia, and R. L. Headrick, Phys. Rev. Lett. **80**, 4713 (1998).
[12] G. Costantini, S. Rusponi, F. B. de Mongeol, C. Boragno, and U. Valbusa, J. Phys.: Condens. Matter **13**, 5875 (2001).
[13] O. Malis, J. D. Brock, R. L. Headrick, M. S. Yi, and J. M. Pomeroy, Phys. Rev. B **66**, 035408 (2002).
[14] S. van Dijken, D. de Bruin, and B. Poelsema, Phys. Rev. Lett. **86**, 4608 (2001).
[15] E. Chason, M. B. Sinclair, J. A. Floro, A. Hunter, and R. Q. Hwang, Appl. Phys. Lett. **72**, 3276 (1998).
[16] R. M. Bradley and J. M. E. Harper, J. Vac. Sci. Technol. A **6**, 2390 (1988).
[17] P. Sigmund, Phys. Rev. **184**, 383 (1969).
[18] C. Herring, J. Appl. Phys. **21**, 301 (1950); W. W. Mullins, *ibid.* **30**, 77 (1959).
[19] R. Cuerno and A. L. Barabasi, Phys. Rev. Lett. **74**, 4746 (1995).
[20] J. Villain, J. Phys. I **1**, 19 (1991);P. Politi and J. Villain, Phys. Rev. B **54**, 5114 (1996).
[21] *ASM Handbook Committee*, *Metals Handbook*, 9th ed. (American Society for Metals, Ohio, 1985), Vol. 9, pp. 48–56.
[22] J. M. Elson, Phys. Rev. B **30**, 5460 (1984).
[23] J. Erlebacher, M. J. Aziz, E. Chason, M. B. Sinclair, and J. A. Floro, J. Vac. Sci. Technol. A **18**, 115 (2000).
[24] D. J. Marwick, SRIM-2000.40, IBM Co., Yorktown, NY, 1984–2000. The penetrating depth of Ar ions for this sputtering condition is estimated to be 16 Å. The Gaussian width of the energy distribution along the ion beam direction and the transverse direction is 9 Å and 11 Å, respectively. The angle of ripples orientation is determined by equating $\nu_x = \nu_y$ using the formula in Ref. 2.
[25] E. Chason, J. Erlebacher, M. J. Aziz, J. A. Floro, and M. B. Sinclair, Nucl. Instrum. Methods Phys. Res. B **178**, 55 (2001).